www.springer.com/41230
https://doi.org/10.1007/s41230-026-4263-x
Research & Development
Vol. 23 No. 6 November 2026
CHINA FOUNDRY

Effect of heat treatment on microstructure and mechanical properties of ZL270LF aluminum alloy

Jia-zhi An[1,2], Jian-ying Sun[1,2], Shi-hao Chen[3], Hao-deng Yuan[1,2], *Wan-wu Ding[1,2], Zhen-zhong Zhang[1,2], and Hai-cun Yu[1,2]

1. School of Materials Science and Engineering, Lanzhou University of Technology, Lanzhou 730050, China

2. State Key Laboratory of Advanced Processing and Recycling of Nonferrous Metals, Lanzhou University of Technology, Lanzhou 730050, China

3. Xian XD Electrical Material Co., Ltd., Xi'an 710000, China

Copyright © 2026 Foundry Journal Agency

Abstract: The effects of different heat treatment processes on the microstructure and mechanical properties of ZL270LF aluminum alloy were studied by metallographic microscope (OM), scanning electron microscope (SEM), backscattered electron diffraction (EBSD), transmission electron microscope (TEM), micro-Vickers hardness, and tensile test. The results show that the hardness, ultimate tensile strength, yield strength, and elongation of ZL270LF aluminum alloy increase from 102 HV, 286 MPa, 173.6 MPa, and 2.3% before heat treatment to 136 HV, 433.4 MPa, 261.9 MPa, and 12.4% after solution at 540 °C for 6 h and aging at 160 °C for 10 h, increasing by 33.3%, 51.4%, 50.8%, and 439.1%, respectively. The average grain size increases from 127.6 μm before heat treatment to 142.9 μm after heat treatment, but the grain size distribution is more uniform. Meanwhile, the $CuAl_2$ phase in ZL270LF aluminum alloy changes into a discontinuous short rod-like distribution from distributing in a network at the grain boundary before heat treatment. Furthermore, La and Ti elements in ZL270LF aluminum alloy are distributed on or near the surface of the second phase particles such as $CuAl_2$, which is one of the main reasons for the improvement of mechanical properties of the alloy during heat treatment.

Keywords: ZL270LF aluminum alloy; heat treatment; $CuAl_2$; microstructure; mechanical property

CLC numbers: TG146.21 **Document code:** A **Article ID:** 1672-6421(2026)06-877-09

1 Introduction

Aluminum alloy is widely used in aerospace, automobile manufacturing, construction engineering, and other fields because of their light weight, high strength, excellent corrosion resistance, durability, and recyclability, etc[1-4]. Al-Cu alloys, characterized by their high strength-to-weight ratio, large modulus-to-weight ratio, good oxidation resistance, and excellent thermal stability, have been found widespread applications in the automotive and aerospace industries[5]. However, improving the mechanical properties of cast Al-Cu alloy products is still a key technical problem to be overcome to ensure low cost and short cycle. Heat treatment is an effective way to improve the mechanical properties of alloys[6]. Therefore, it is of great significance to explore the effect of different heat treatment parameters on the microstructure and properties of Al-Cu alloy.

In recent years, a series of related research on the heat treatment of Al-Cu alloys has been carried out. Zhu et al.[7] pursued the efficacy of aging time and aging temperature on the mechanical properties of Al-Cu alloys. It was concluded that by increasing the aging temperature, tensile and yield strengths firstly enhanced and then decreased. Nevertheless, both yield strength and tensile strength were improved by extending the aging time. Çetintürk et al.[8] thoroughly examined the influence of various inoculant types such as $AlSr_{10}$, Al_3TiB, and Al_5TiB, along with T6 heat treatment, on the microstructure, mechanical properties, and corrosion behavior of Al-5%Cu alloy. The outcomes revealed that the Al-5%Cu with 5% Ti addition exhibited the finest grains in the structure.

***Wan-wu Ding**

Male, 1979, Ph. D., Researcher. His research interests mainly focus on strengthening and toughening of aluminum alloys, and comprehensive utilization of metallurgical solid waste resources.

E-mail: dingww@lut.edu.cn

Received: 2024-11-28; Revised: 2025-01-06; Accepted: 2025-01-08

In this respect, hardness, tensile strength, and wear resistance were systematically enhanced as the grain size decreased.

According to the research of Jang et al.[9], the mechanical properties of Al-Cu alloy firstly increased and then decreased with the increase of solution temperature. Compared with solution temperature, solution time had a small influence on the microstructure and mechanical properties of Al-Cu alloy. In addition, the ultimate tensile strength increased with the increase of aging time and temperature when the artificial aging treatment was carried out at 160–180 °C for 2–8 h. Meanwhile, it was also found that the yield strength has the same trend with ultimate tensile strength.

Squeeze-cast Al-Cu alloys develop four θ-series precipitates during aging: Guinier-Preston (GP) zones, θ'' (Al_3Cu), θ' ($CuAl_2$), and θ ($CuAl_2$) phases. Among these, θ'' phases provide optimal strengthening effect due to their fully coherent interfaces with the α-Al matrix, followed by GP zones and θ' phases, while the incoherent θ-phase exhibits markedly diminished contributions[10]. Introducing lithium into Al-Cu alloys followed by T6 tempering promotes the formation of sub-micron T-phase ($Al_{20}Mn_3Cu_2$), nano-scale T1 (Al_2CuLi), and ultrafine θ' ($CuAl_2$) precipitates. These phases maintain coherent/semi-coherent crystallographic relationships with the matrix, effectively suppressing strain localization and fracture initiation while significantly enhancing strength[11]. Furthermore, homogeneous dispersion of nano-scale Al_6MnCu and θ'' precipitates within the matrix synergistically contributes to precipitation strengthening, achieving concurrent improvements in both strength and ductility[12].

ZL270LF aluminum alloy is one of the representatives of high-performance Al-Cu casting alloys, which is developed in recent years and has been gradually applied to important automotive lightweight structural parts. However, the heat treatment parameters are difficult to choose because of the high alloying degree of ZL270LF aluminum alloy. During the heat treatment process, the surface cracks, adiabatic shear bands, and uneven grain distribution often occur if the process parameters do not match[13, 14]. It has been pointed out that the microstructural evolution of Al-Cu alloy ingots is strongly influenced by the heat treatment and subsequent deformation conditions[9]. In addition, ZL270LF aluminum alloy contains a small amount of rare earth elements (La, Ce). Relevant studies[15] indicate that the rare earth element La can effectively inhibit the growth of the $CuAl_2$ phase during the solidification process. However, research on the inhibitory effect of rare earth elements on the θ ($CuAl_2$) phase during heat treatment has been less extensively studied. Therefore, it is necessary to study the heat treatment process of ZL270LF aluminum alloy and its influence on the microstructure and mechanical properties of the alloy.

In this study, the effect of different heat treatment processes on the properties and microstructure of ZL270LF aluminum alloy was investigated to identify the optimal heat treatment process parameters. Additionally, the influence of microstructural changes induced by heat treatment on the alloy's properties was explored. The present research will provide the theoretical basis for the subsequent engineering application of ZL270LF aluminum alloy.

2 Experimental materials and methods

The ZL270LF aluminum alloy was provided from Gansu Hongda Aluminum Profile Co., Ltd., with cylindrical ingots measuring Φ225 mm×1,500 mm. The main chemical composition is listed in Table 1, wherein the total content of rare earth elements (La/Ce) was 0.1wt.%.

The thermal analysis of ZL270LF aluminum alloy was carried out by differential scanning calorimetry (DSC). The melting temperature of low melting point eutectic phase was identified to determine the solid solution temperature. Figure 1 shows the DSC thermal analysis curve of ZL270LF aluminum alloy. It can be seen that the first peak appears at 535 °C, indicating that the second phase of ZL270LF aluminum alloy occurs in solid solution at about 535 °C, that is, the strengthening phase $CuAl_2$ begins to dissolve into the matrix at about 535 °C.

Table 1: Main components of ZL270LF aluminum alloy (wt.%)

Cu	Mn	Mg	Si	Ti	Re	RE	Al
4.730	0.777	0.603	0.395	0.191	0.018	0.1	Bal.

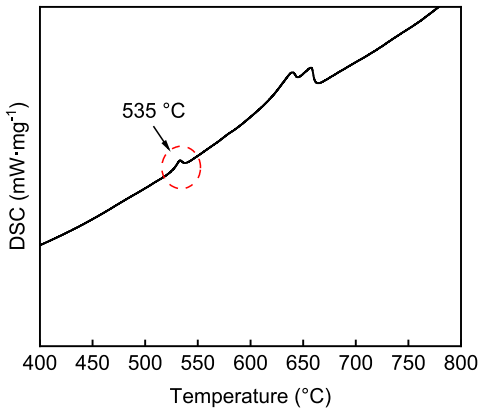


Fig. 1: DSC curve of ZL270LF aluminum alloy

To investigate the impact of different solution temperatures on the properties of the alloy, the solution treatments were conducted at 530 °C (A1–A4), 535 °C (B1–B4), 540 °C (C1–C4), a holding for 6 h followed by water quenching. In the present study, an aging temperature of 160 °C was selected, and the holding time of 6 h, 8 h, 10 h, and 15 h were chosen to determine the optimal heat treatment parameters of the alloy because the aging temperature of Al-Cu alloy generally ranged from 155 °C to 170 °C[15], and the aging time varied from 4 h to 16 h. The sample size for heat treatment was 150 mm×50 mm×50 mm. KSL-1400X Muffle furnace was selected as the solid solution equipment, and DGG-9146A constant temperature drying oven was used for aging treatment after water quenching. The specific heat treatment parameters are shown in Table 2.

Table 2: Specific heat treatment parameters of ZL270LF aluminum alloy

Samples	Solution treatment	Aging treatment
A0	/	/
A1	530 °C×6 h	160 °C×6 h
A2		160 °C×8 h
A3		160 °C×10 h
A4		160 °C×15 h
B1	535 °C×6 h	160 °C×6 h
B2		160 °C×8 h
B3		160 °C×10 h
B4		160 °C×15 h
C1	540 °C×6 h	160 °C×6 h
C2		160 °C×8 h
C3		160 °C×10 h
C4		160 °C×15 h

The hardness test samples with dimension of 10 mm×10 mm×10 mm were taken from the samples. The hardness test was carried out on the WILSON VH1102 micro-Vickers hardness tester after grinding and polishing. Seven points were tested for each sample, and the average value was taken as the final result. The tensile samples were processed according to GBT 228.1-2010 standard, as shown in Fig. 2, and the tensile test was carried out on the MTS tensile tester at room temperature with a tensile speed of 0.1 mm·min^{-1}. The mechanical property data of the samples during stretching were collected using an extensometer. In order to ensure the accuracy of the mechanical properties data of the alloy, the tensile tests were repeated at least three times. The metallographic structure of the sample was observed with a Zeiss LSM 800 laser local microscope after the electrolytic etch (alcohol: perchloric acid product ratio is 9:1). The microstructure and tensile fracture of the alloy were observed and analyzed with the XJ-800FS scanning electron microscope produced by Simak Mayer. The microstructure was further observed with the FEI Talos F200X transmission electron microscope produced by the FEI company.

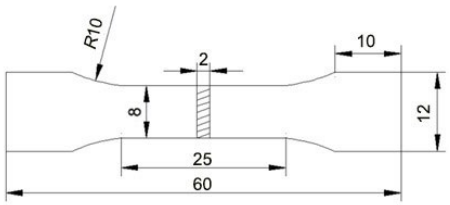


Fig. 2: Size of standard tensile specimen (unit: mm)

3 Results and discussion

3.1 Mechanical properties of ZL270LF aluminum alloy under different heat treatments

Figure 3 shows the stress-strain curves of samples. Table 3 shows the statistical results of hardness, ultimate tensile strength (UTS), yield strength (YS), and elongation of ZL270LF aluminum alloy under different heat treatment processes. In this investigation, the quality index (Q) was employed to quantify the comprehensive mechanical properties of aluminum alloys, following the established formulation Q=UTS+$a$log(elongation%)[16], where the value of a is usually 150 for aluminum alloys[16]. When the heat treatment parameters of ZL270LF aluminum alloy are 540 °C×6 h+160 °C×10 h (Sample C3), the value of the quality index Q is 597.4 MPa, which is the largest value and indicating the best comprehensive performance.

The hardness, ultimate tensile strength, yield strength, and elongation of A0 sample increase from 102 HV, 286 MPa, 173.6 MPa, and 2.3% to 136 HV, 433.4 MPa, 261.9 MPa, and 12.4% of C3, increasing by 33.3%, 51.4%, 50.8%, and 439.1%, respectively.

To systematically investigate the microstructural evolution (the second-phase particles, microstructure, and fracture morphology) of ZL270LF aluminum alloy during heat treatment, comparative analysis was conducted between the as-cast sample (A0) and the best comprehensive performance sample (C3) after heat treatment.

3.2 Microstructure analysis of ZL270LF aluminum alloy

Figure 4 shows the XRD patterns of as-cast A0 and heat-treated

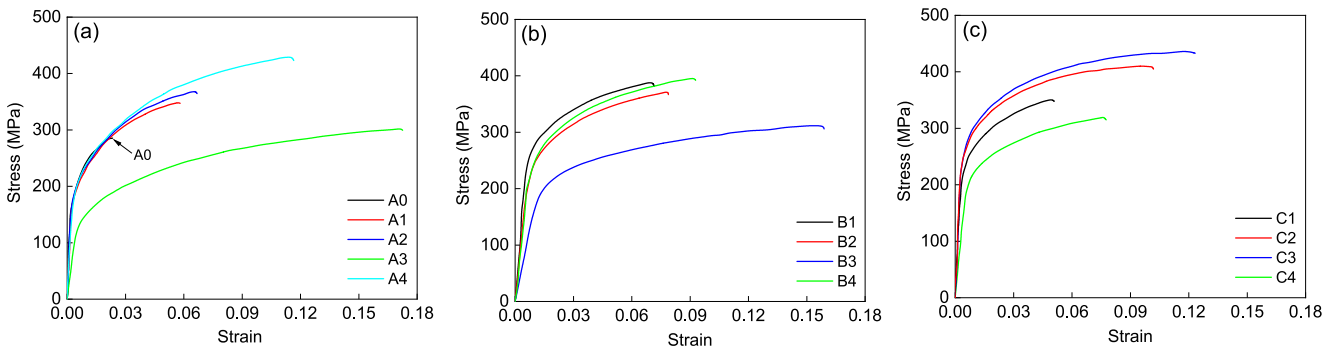


Fig. 3: Engineering stress-strain curves of samples: (a) A0–A4; (b) B1–B4; (c) C1–C4

Table 3: Statistical of mechanical properties of different samples

Samples	Hardness (HV)	UTS (MPa)	YS (MPa)	Elongation (%)	Q
A0	102.0	286.0	173.6	2.3	340.3
A1	127.3	348.1	175.9	5.8	462.6
A2	138.0	368.2	192.3	6.7	492.1
A3	156.3	302.1	140.8	17.3	487.8
A4	142.4	429.8	188.5	11.6	589.5
B1	117.5	387.2	258.2	7.0	514.0
B2	137	372.7	231.1	7.9	507.3
B3	153.3	313.8	204.2	15.9	494.0
B4	146.3	396.1	238.9	9.3	541.4
C1	126.6	352.6	244.9	5.0	457.4
C2	134.4	409.8	248.4	10.1	560.4
C3	136.0	433.4	261.9	12.4	597.4
C4	118.1	321.9	218.2	7.7	454.9

C3 ZL270LF aluminum alloy samples. It can be seen that the main phases of A0 and C3 samples in ZL270LF aluminum alloy are α-Al and $CuAl_2$. The $CuAl_2$ is the main strengthening phase, which can improve the mechanical properties of the alloy by solution strengthening and age hardening[17]. Comparing the diffraction peak strength of $CuAl_2$ in Fig. 4, it can be found the $CuAl_2$ phase peak in the C3 sample exhibits a significant decrease, suggesting that this phase is predominantly dissolved into the α-Al matrix following heat treatment.

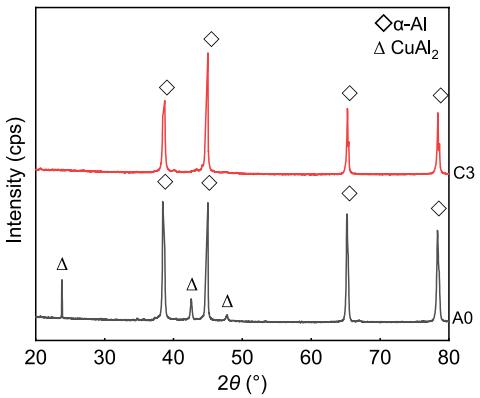


Fig. 4: XRD patterns of as-cast A0 and heat-treated C3 ZL270LF aluminum alloy samples

Figure 5 shows the macroscopic microstructure, EBSD microstructure, and grain size distribution of A0 and C3 samples. It can be seen from Fig. 5 that the C3 specimen still exhibits a fine equiaxed grain structure. The number of grain sizes above 150 μm decreases significantly after heat treatment although the average grain size increases from 127.6 μm in the as-cast state to 142.9 μm in the heat-treated state. The grain distribution after heat treatment is more concentrated than that before heat treatment, mainly because Cu dissolves into the aluminum matrix and forms a supersaturated solid solution during the high-temperature solution stage[18]. Some Cu are precipitated from the aluminum matrix and form a fine precipitated phase during the aging process. In addition, the heat treatment makes the grain boundary migration and degradation, resulting in grain growth[19]. A homogeneous grain structure reduces stress gradients at grain boundaries, enabling more uniform stress distribution within the material matrix, and thereby suppressing crack nucleation and propagation, therefore improving the fatigue resistance and stability of ZL270LF aluminum alloy.

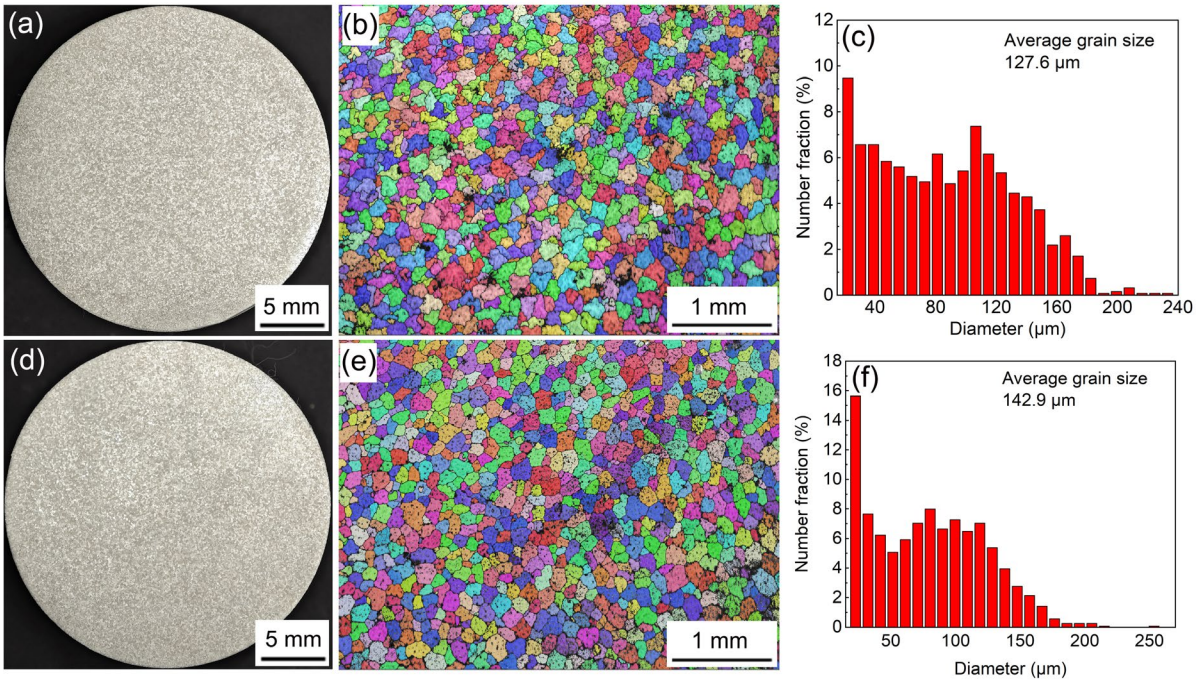


Fig. 5: Microstructure, EBSD, and grain size distribution of as-cast A0 (a–c) and heat-treated C3 (d–f) ZL270LF aluminum alloy

Figure 6(a) reveals that the as-cast ZL270LF aluminum alloy predominantly comprises a gray α-Al matrix and bright-white secondary phases. These bright-white secondary phases are primarily distributed along grain boundaries, exhibiting a continuous network morphology in Fig. 6(b). Additionally, discrete black secondary phase particles are observed within the α-Al matrix. According to EDS analysis in Figs. 6(c–f) and Table 4, these black particles are mainly rich in Mn and Al elements. It can be seen from Table 4 that the white second phase is mainly composed of Al and Cu elements, and the ratio of Al and Cu elements is close to 2:1. Combined with XRD analysis, the bright white second phase in as-cast ZL270LF aluminum alloy is $CuAl_2$ phase. In addition, there are black particles with a diameter of about 3 μm near the $CuAl_2$ phase. According to the element proportion, these black particles are believed to be formed by the enrichment of alloying elements such as Mn in ZL270LF aluminum alloy around the $CuAl_2$ phase.

Figure 7 shows the TEM structure images of the as-cast ZL270LF aluminum alloy. There are some irregular particles inside the grain, which are mainly concentrated near the grain boundaries. According to the results of selective regional electron diffraction (SAED) in Region B, these particles are mainly α-Al. However, the particles present a shell and wrapped structure as the particles are further enlarged. The granular secondary phase particles encapsulated by these shell-like structures inhibit their growth and act as an additional barrier to dislocation motion, thereby playing a significant role in enhancing the mechanical properties of the alloy.

In order to further observe the composition of the granular secondary phase particles encapsulated by these shell-like structures, the microstructure and EDS analysis are shown in Fig. 8. According to the STEM-HAADF image and surface scanning distribution of the particles in Fig. 8, the outer layer structure of the second phase particles is mainly a binary eutectic phase of α-Al+$CuAl_2$, and the inner layer is a ternary eutectic phase of α-Al+$CuAl_2$+$Al_{20}Cu_2Mn_3$[20]. Meanwhile, La and Ti elements are distributed near the particles which inhibit the excessive growth of these second phase particles, thus forming nano-scale particles. These fine second phase particles can play a pining effect on subgrain boundaries and grains during plastic deformation to inhibit dynamic recrystallization[21], thereby increasing the recrystallization temperature and retaining the dislocation generated during deformation. The ultimate tensile strength and yield strength of the as-cast ZL270LF alloy increase by 40.36% and 199%, respectively, compared to the rare-earth-free Al-5Cu as-cast alloy (175 MPa, 58 MPa)[22].

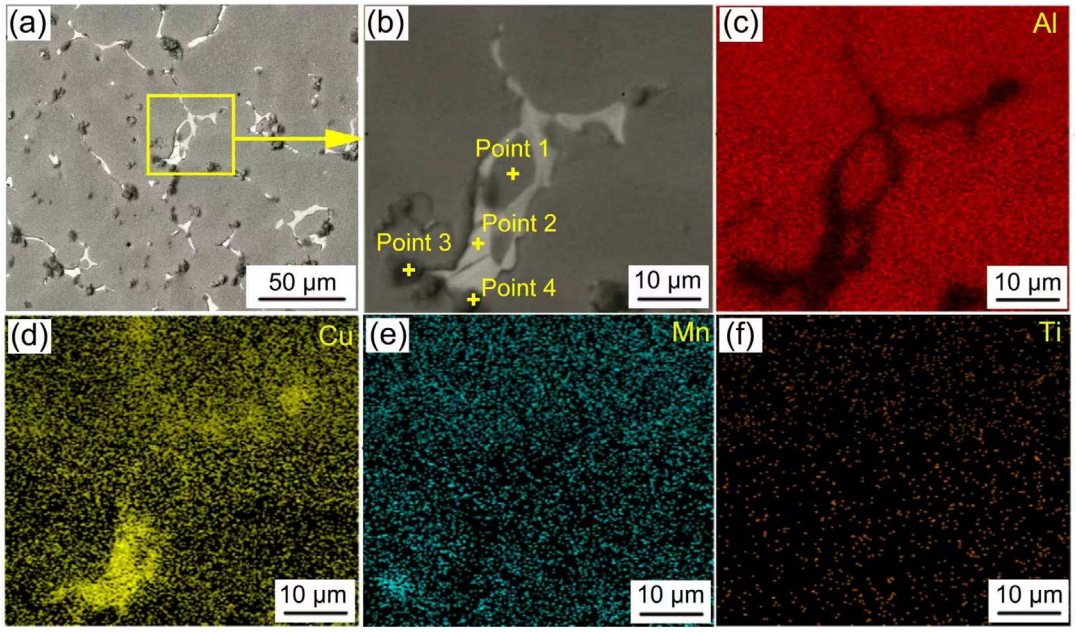


Fig. 6: SEM and EDS analysis of as-cast ZL270LF aluminum alloy: (a–b) SEM images; (c–f) surface scan distribution mapping of Al, Cu, Mn, and Ti elements

Table 4: EDS results of each point in Fig. 6(b) (mass fraction, %)

Point	Al	Cu	Mn	Type of second phase
1	92.3	7.4	0.2	α-Al
2	67.1	31.1	1.2	$CuAl_2$
3	79.4	3.9	16.4	Containing Mn
4	86.2	5.1	8.7	Containing Mn

Figure 9 shows the TEM images of the precipitated phase, the diffraction spots, and their corresponding crystal plane spacing of C3 sample. It can be seen from Fig. 9 that typical needle-like θ' phases precipitate on the matrix of ZL270LF aluminum alloy after heat treatment, and θ' phases are perpendicular to each other, which have a size of about 50–100 nm. In addition, short rod-like second phases are found on the grain boundary, which can be identified as $CuAl_2$ by diffraction spots and crystal face spacing.

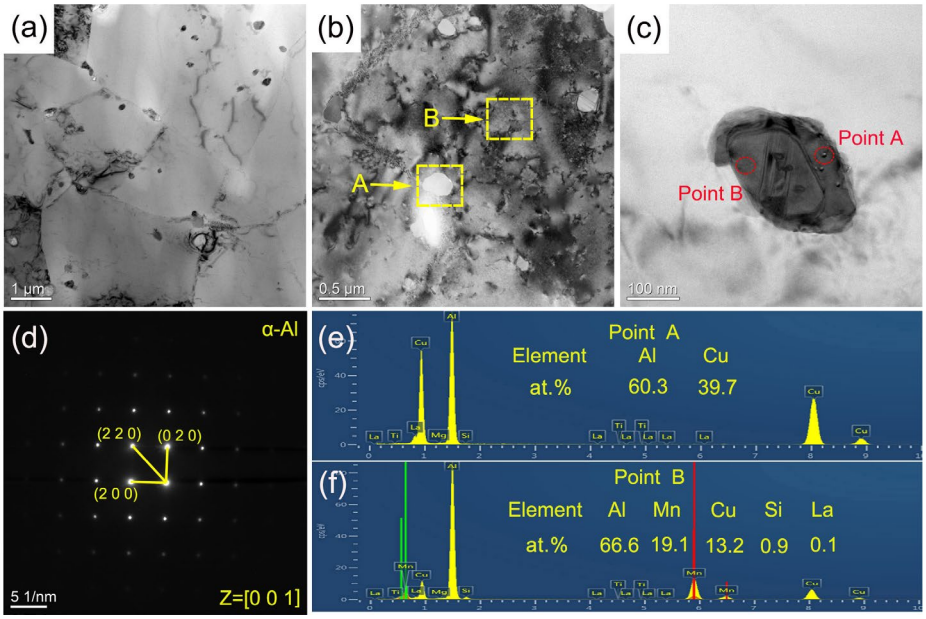


Fig. 7: TEM structure of as-cast ZL270LF aluminum alloy: (a–b) morphology of particles; (c) an enlarged view of Region A in (b); (d) SAED of Region B in (b); (e–f) EDS analysis in (c)

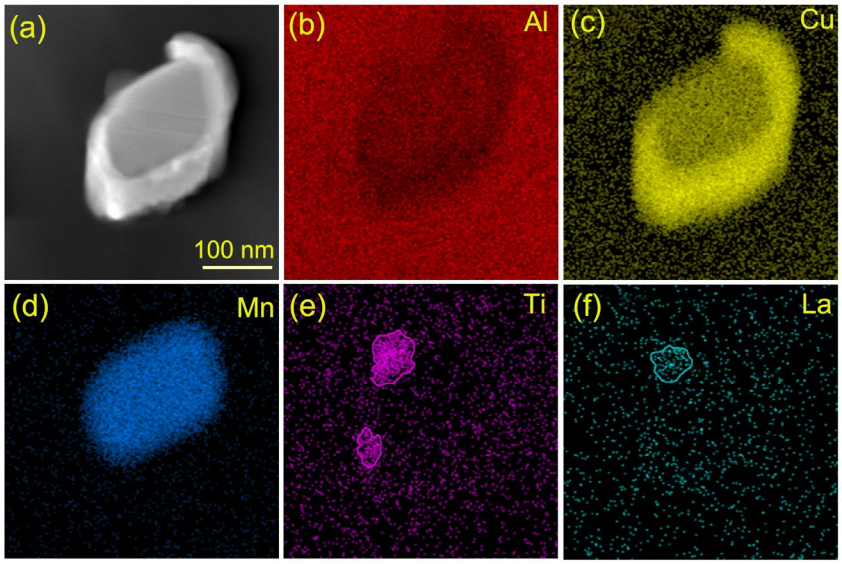


Fig. 8: STEM-HAADF image of second-phase particles (a) and surface scanning distribution mappings of Al, Cu, Mn, Ti, and La elements (b–f)

Compared Fig. 9(a) with Fig. 6(b), it can be seen that the morphology of $CuAl_2$ changes significantly from a continuous network distribution at the grain boundary in the as-cast state to a short rod-like shape after heat treatment, which may be caused by recrystallization and growth of the grains, forming larger and more ordered grains. This recrystallization may result in the transformation from network structure into a larger rod-like structure of $CuAl_2$[23]. In addition, the heat treatment process may change the crystal structure, therefore changing the distribution of $CuAl_2$. In the solution stage, the $CuAl_2$ dissolves into the aluminum matrix, forming a supersaturated solid solution. During the aging process, the $CuAl_2$ precipitates from the aluminum matrix at the grain boundaries with a more stable structure because the atoms rearrange.

Figure 10 shows the SEM and EDS analysis of $CuAl_2$ at the grain boundary of the C3 sample. A small amount of rare earth elements La and Ti are attached to the surface of short rod-like $CuAl_2$ phase. Furthermore, the La and Ti can inhibit the excessive growth of $CuAl_2$ during heat treatment by attaching to the outer layer of the $CuAl_2$ phase. Additionally, Ti elements also adhere to the $CuAl_2$ phase, enabling the transformation of the as-cast micron-scale, continuously network $CuAl_2$ phase (Fig. 6) into discrete, nanoscale rod-shaped precipitates (approximately 300 nm, Fig. 9).

Meanwhile, a granular second phase is also found inside the grain of the C3 sample, as shown in Fig. 11. Through surface scanning analysis of the particle, it can be identified that the black granular phase is a ternary eutectic phase composed of Al, Cu, and Mn. There are small amounts of rare earth elements La and Ce in these second-phase particles, as shown in Figs. 11(e) and (f). La and Ce adsorb on the surface of the second phase particles such as $CuAl_2$, preventing the growth

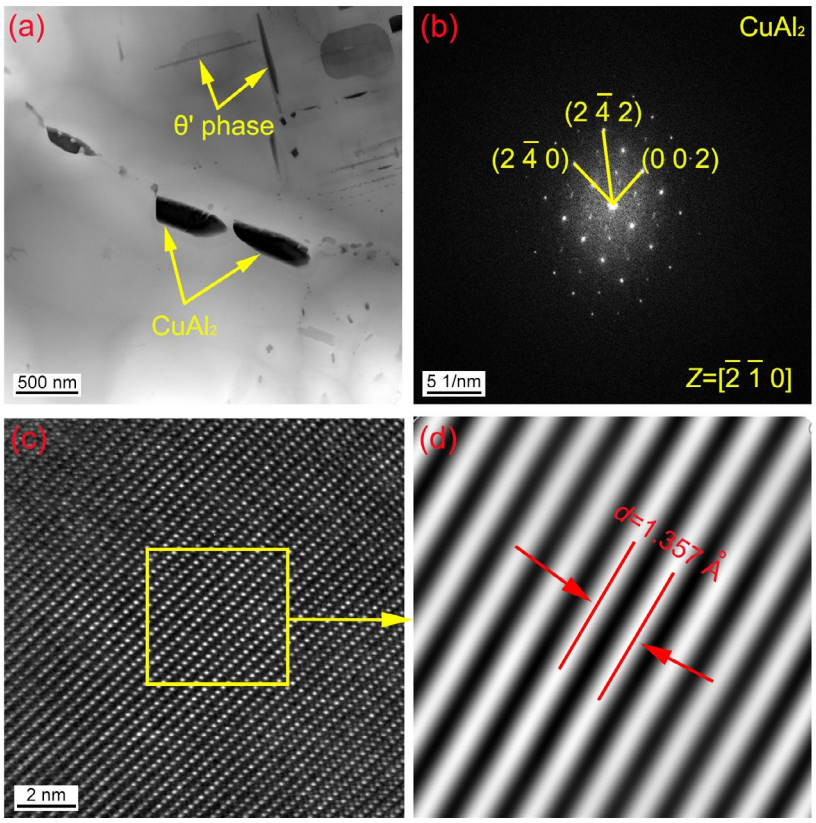


Fig. 9: TEM images of precipitates in C3 samples: (a) morphology of $CuAl_2$ and θ' phases; (b) diffraction spots of $CuAl_2$; (c–d) crystal face spacing of $CuAl_2$

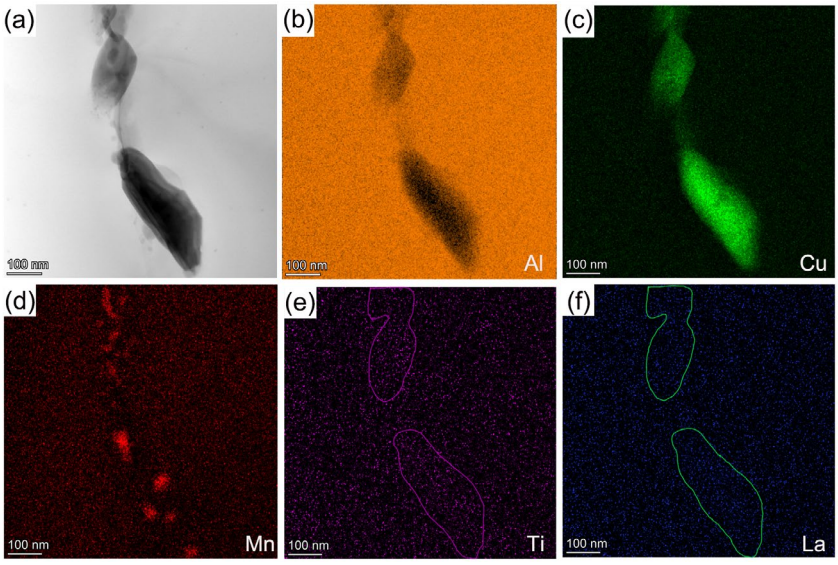


Fig. 10: Surface scan image of $CuAl_2$ at grain boundaries of C3 sample: (a) $CuAl_2$ phase; (b–f) area scanning distribution maps of Al, Cu, Mn, Ti, and La elements

of these second phase particles. Ce is preferentially gathered at grain boundaries in liquid aluminum due to its strong chemical activity, which can reduce the distribution coefficient of Cu, therefore effectively inhibiting the growth of columnar crystals and promoting the formation of fine equiaxed grains[24], as shown in Fig. 5(d). Xiao et al.[25] presented that the addition of Ce can reduce the segregation of Cu on the grain boundary, and increase the precipitation density of the phase, thereby enhancing the precipitation strengthening effect of θ'. In addition, Liao et al.[26] found that 0.1wt.% addition of La and Ce does not alter the solidification microstructure besides the formation of small amount of La- or Ce-rich intermetallic compounds. It was reported that the addition of 0.2wt.% La or Ce could provide heterogenous nucleation sites for the α-Al phase and suppress its growth[27]. In summary, rare earth elements La and Ce can be effectively utilized to promote the growth of equiaxed grains and inhibit the coarsening of the $CuAl_2$ phase during casting and heat treatment processes.

The $CuAl_2$ phase exhibits significant mechanical enhancement through dual strengthening mechanisms: solid solution

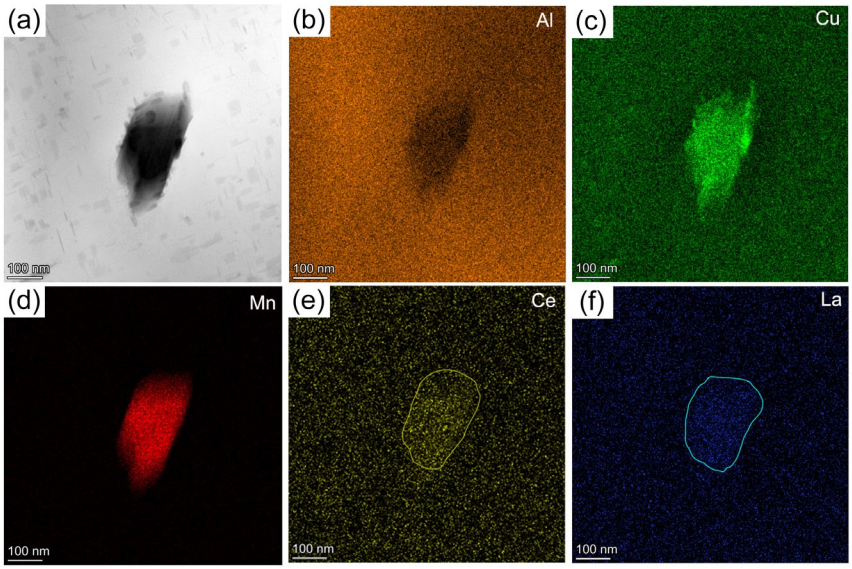


Fig. 11: Transmission electron microscopy image of granular second phase after heat treatment: (a) TEM map; (b–f) surface scan distribution of Al, Cu, Mn, Ce, and La elements

strengthening via solute atom-induced lattice distortion, and precipitation hardening during aging treatment. Post-heat treatment microstructural analysis reveals that the initial as-cast continuous network $CuAl_2$ transforms into discrete rod-shaped precipitates. Concurrently, Cu segregation at grain boundaries decreases, effectively mitigating grain boundary embrittlement. This morphological transition, contrasted with crack-susceptible coarse networks in conventional cast alloys, enhances crack resistance through precipitate-boundary interactions. Furthermore, grain size homogenization reduces stress gradients at grain boundaries, promoting homogeneous load transfer.

3.3 Fracture analysis of ZL270LF aluminum alloy

Figure 12 shows the fracture morphology of ZL270LF aluminum alloy before and after heat treatment. The as-cast ZL270LF aluminum alloy exhibits a predominantly intergranular fracture mode, characterized by cleavage planes and facets. This is because the network $CuAl_2$ phase in the as-cast state is easy to cause a brittle fracture in the matrix, thereby resulting in a brittle fracture morphology. The fracture morphology of ZL270LF aluminum alloy after heat treatment changes from cleavages to a dimple with a diameter of about 2 μm, which is a typical ductile fracture. This phenomenon primarily arises from the dissolution of the as-cast networked $CuAl_2$ phase during heat treatment, which contributes to solid solution strengthening. Simultaneously, the formation of rod-shaped nanoscale $CuAl_2$ precipitates provide precipitation hardening, thereby improving the plasticity and toughness of the ZL270LF aluminum alloy. Therefore, ZL270LF aluminum alloy after heat treatment exhibits higher elongation and tensile strength. In summary, ZL270LF aluminum alloy has the characteristics of brittle fracture in the as-cast state, but its toughness is significantly improved after heat treatment.

4 Conclusions

In this study, the microstructure and properties of ZL270LF aluminum alloy before and after heat treatment were studied. The main conclusions are as follows:

(1) The optimal heat treatment process of as-cast ZL270LF aluminum alloy is 540 °C×6 h (solution)+160 °C×10 h (aging). The hardness, ultimate tensile strength, yield strength, and elongation of ZL270LF aluminum alloy increase significantly from 102 HV, 286 MPa, 173.6 MPa, and 2.3% in the as-cast sample to 136 HV, 433.4 MPa, 261.9 MPa, and 12.4% after optimal heat treatment, respectively.

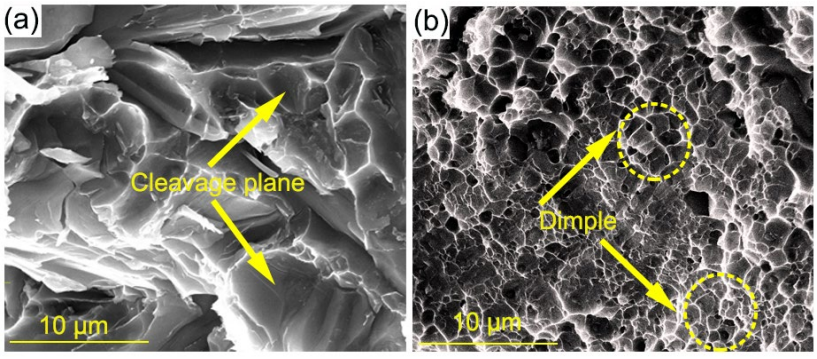


Fig. 12: Fracture morphology of ZL270LF aluminum alloy: (a) as-cast; (b) heat treated

(2) The average grain size of ZL270LF aluminum alloy increases from 127.6 μm in the as-cast state to 142.9 μm under the optimal heat treatment process, but the grain size distribution is relatively concentrated and the grain sizes are more uniform.

(3) Optimal heat treatment changes the large-sized network $CuAl_2$ into a short rod or granule in the ZL270LF aluminum alloy. The La and Ti elements are distributed on or near the surface of the second phase particles such as $CuAl_2$, which effectively inhibits their overgrowth during heat treatment.

(4) The as-cast ZL270LF aluminum alloy is mainly characterized by an intergranular fracture with obvious cleavage planes and cleavage facets, which is a typical brittle fracture. After heat treatment of 540 °C×6 h+160 °C×10 h, the fracture morphology of ZL270LF aluminum alloy changes from cleavage facets to the fine dimples, indicating a ductile fracture mode.

Acknowledgments

This work was supported by the National Natural Science Foundation of China (52161006), the Industrial Support Plan Project of Gansu Provincial Department of Education (2021CYZC-23), the Central Guidance for Local Scientific and Technological Development Funding Projects (23ZYQB309), the Gansu Provincial Science and Technology Major Project (22ZD6GB019), and the Lanzhou Youth Science and Technology Talent Innovation Project (2024-QN-106).

Conflict of interest

The authors declare that they have no known competing financial interests or personal relationships that could have appeared to influence the work reported in this paper.

References

[1] Zheng Y Y, Luo B H, Xie W, et al. Microstructure evolution and precipitation behavior of Al-Mg-Si alloy during initial aging. China Foundry, 2023, 20(1): 57–62.
[2] Li J, Lü S, Wu S, et al. Micro-mechanism of simultaneous improvement of strength and ductility of squeeze-cast Al-Cu alloy. Materials Science and Engineering: A, 2022, 833: 142538.
[3] Xue H, Chen T J, Zhang X Z, et al. Effect of mixing temperature on microstructure of an Al-Si alloy prepared by controlled diffusion solidification. China Foundry, 2023, 20(3): 241–252.
[4] Nikzad M H, Motamedi M, and Nasri M R. Enhancement of mechanical properties of Al-Cu alloy composite reinforced by Ni element: A combination of mixture design of experiment and artificial neural network approach. Material Today Communications, 2024, 38: 107902.
[5] Gao C, Zhang B R, Li Y M, et al. Synergistic effect of Zr and Mo on precipitation and high-temperature properties of Al-Si-Cu-Mg alloys. China Foundry, 2024, 21(1): 71–81.
[6] Li X. Mechanical properties of aluminum alloys under low-cycle fatigue loading. Materials, 2019, 12(13): 2064.
[7] Zhu X, Lin Y, Wu Q, et al. Effects of aging on precipitation behavior and mechanical properties of a tensile deformed Al-Cu alloy. Journal of Alloys and Compounds, 2020, 843: 155975.
[8] Çetintürk S, Tarakçioğlu N, Acarer M, et al. Using quadratic multiple linear regression models to investigate the effect of inoculant type and T6 heat treatment on microstructural, mechanical and corrosion properties of Al-Cu alloy produced by casting. Material Today Communications, 2023, 35: 105549.
[9] Jang J H, Nam D G, Park Y H, et al. Effect of solution treatment and artificial aging on microstructure and mechanical properties of Al-Cu alloy. Transactions of Nonferrous Metals Society of China, 2013, 23: 631–635.
[10] Liu H, Papadimitriou I, Lin F X, et al. Precipitation during high temperature aging of Al-Cu alloys: A multiscale analysis based on first principles calculations. Acta Materialia, 2020, 167: 121–135.
[11] Li J Y, Pan Y, Wu S S, et al. Precipitates strengthening mechanism of a new squeeze-cast Al-Cu-Li-Mn alloy with high strength and ductility. Journal of Materials Research and Technology, 2023, 25: 1334–1343.
[12] Li J Y, Lü S L, Wu S S, et al. Micro-mechanism of simultaneous improvement of strength and ductility of squeeze-cast Al-Cu alloy. Materials Science & Engineering: A, 2022, 833: 142538.
[13] Zhang H, Huang L, Wang W, et al. Mechanical behavior and fracture mechanism of 2219 aluminum alloy under dynamic loading at different heat treatment states. Rare Metal Materials and Engineering, 2022, 51: 2560–2569.
[14] Zhu X, Fan Q, Wang D, et al. A new dynamic recrystallization mechanism in adiabatic shear band of an α/β dual phase titanium alloy: Composition redistribution. Scripta Materialia, 2024, 206: 114229.
[15] Yang M. Heat treatment process parameter manual. China Machine Press, 2013. (In Chinese)
[16] Tiryakiolu M, Campbell J, and Alexopoulos N D. Quality Indices for aluminum alloy castings: A critical review. Metallurgical and Materials Transactions: B, 2009, 40: 802–811.
[17] Fu K Y, Zhu D X, Zhang Y Q, et al. Predictive modeling of tensile strength in aluminum alloys via machine learning. Materials, 2023, 16: 7236.
[18] Wang W and Liu B. Roles of the semisolid heating on the microstructure of a hypereutectic Al-Fe-Cu alloy. Scientific Reports, 2021, 11: 1–14.
[19] Wisz G, Paulina S, Maciej S, et al. Formation and characterization of stable TiO_2/Cu_xO-based solar cells. Materials, 2023, 16: 5683.
[20] Yu F, Xu D, Chen S, et al. Effect of Cu content on anisotropy of mechanical property of Al-Cu-Mn alloy. Chinese Journal of Materials Research, 2018, 32: 853–860. (In Chinese)
[21] Wang C, Zhang J, Yi Y, et al. Effect of pretreatment and cryogenic temperatures on mechanical properties and microstructure of Al-Cu-Li alloy. Materials, 2021, 14: 4873.
[22] Li J, Lin C, Xiao C, et al. Effects of Ce on microstructures and properties of Al-5Cu alloy. Special Casting & Nonferrous Alloys, 2023, 43(11): 1540–1544. (In Chinese)
[23] Chen S. Hot deformation behavior and microstructure evolution of ZL270LF aluminum alloy. Lanzhou: Master's Dissertation, Lanzhou University of Technology, 2023. (In Chinese)
[24] Tian W, Hu M, Sun Y, et al. Research progress on effects of rare earth elements on properties of aluminum-copper alloys. Transactions of Materials and Heat Treatment, 2019, 40(3): 12–19. (In Chinese)
[25] Xiao D H, Wang J N, Ding D Y, et al. Effect of rare earth Ce addition on the microstructure and mechanical properties of an Al-Cu-Mg-Ag alloy. Journal of Alloy and Compounds, 2003, 352: 84–88.
[26] Liao H, Lu L, Li G, et al. Influence of minor addition of La and Ce on the ageing precipitation behavior of Sr-modified Al-7Si-0.6Mg alloy. Material Today Communications, 2024, 39: 108825.
[27] Jiang W, Fan Z, Dai Y, et al. Effects of rare earth elements addition on microstructures, tensile properties and fractography of A357 alloy. Materials Science and Engineering: A, 2014, 597: 237–224.